

Optical deformation potentials for PbSe and PbTe

I. I. Zasavitskii,¹ E. A. de Andrada e Silva,² E. Abramof,² and P. J. McCann³

¹*P. N. Lebedev Physical Institute of RAS, Leninskii Pr. 53, 119991 Moscow, Russia*

²*Instituto Nacional de Pesquisas Espaciais—INPE, CP515, 12201-970 Sao Jose dos Campos-SP, Brazil*

³*School of Electrical and Computer Engineering, University of Oklahoma, Norman, Oklahoma 73019, USA*

(Received 20 January 2004; revised manuscript received 24 May 2004; published 8 September 2004)

The values of optical deformation potentials (D_u and D_d) for PbSe and PbTe are analyzed using absorption, luminescence and x-ray diffraction data on high quality, deep quantum well PbSe/PbSrSe and PbTe/PbEuTe structures. Published optical data on PbTe/BaF₂ structures were also used. It is important for these evaluations to use the value of isotropic deformation potential (D_{iso}) which is determined from the low temperature hydrostatic pressure experiments and the intervalley splitting which was determined from differential absorption spectroscopy. The fitting procedure was done using an accurate $\mathbf{k} \cdot \mathbf{p}$ model for the band structure near the fundamental gap including anisotropy, multivalley, and band nonparabolicity effects. Photoluminescence was measured in pulsed mode at 4 and 77 K, which gives the lowest energy state in the rectangular well. The strain and well parameters were measured with a high resolution x-ray diffractometer. We find the new optical deformation potential values at low temperatures: $D_u = -0.2$ and -0.5 eV, and $D_d = 5.3$ and 3.5 eV for PbSe and PbTe, respectively.

DOI: 10.1103/PhysRevB.70.115302

PACS number(s): 78.66.Li, 78.55.Hx, 78.20.Ci, 71.70.Fk

I. INTRODUCTION

There is a considerable interest in studying the energy spectrum changes due to strain in semiconductor multi-quantum well (MQW) heterostructures. It is especially important in the case of IV–VI semiconductors because good lattice matching is restricted to four-component solid solutions and in view of the lack of good substrates, particularly for PbSe. As a result, the most common IV–VI MQW structures are strained and energy spectra depend on the strain and deformation potential values, which in turn are not well known for the Pb salts, the main family of IV–VI semiconductor compounds. In particular, the deformation effects due to uniaxial strain have not been extensively studied. So far, the theoretically and experimentally determined deformation potentials are spread over a wide range; in the case of p -type PbTe, for example, the obtained acoustic potential values vary from 6 to 40 eV.¹ IV–VI semiconductors are soft materials with easy dislocation glide in the $\langle 110 \rangle$ directions along the $\{100\}$ planes,² therefore it is rather difficult to produce uniaxial strain in them directly. In fact, there has been very little work in this area following the pioneering optical studies of Pratt and McMullin³ where uniaxial pressures up to 150 bar produced a spectral shift of 2.5 meV in the low temperature photoluminescence spectra of PbSe crystals. Another way of generating uniaxial strain in heterostructures is to grow lattice-mismatched layers and/or to change the temperature of structures grown on substrates with different thermal expansion coefficients. As optical experiments have shown, the elastic strains in this case result in noticeable spectral changes (up to 20 meV or $\sim 10\%$ of the energy gap).

Spectral changes between free and strained IV–VI epitaxial films were detected in magneto-optical absorption as first reported in Ref. 4. The authors used their results to calculate the interband deformation potential values for the IV–VI semiconductors (see Table IV below). Further magneto-

optical studies of epitaxial films⁵ and superlattices⁶ allowed determination of the deformation potential constants for PbTe using a fitting procedure with many unknown band parameters. Recently, somewhat different values for PbTe^{7–11} and PbSe^{8,12} have been obtained from photoluminescence (PL) and absorption measurements of MQW structures. Similar optical deformation potential values for PbSe were obtained from photoluminescence measurements of PbSe/PbEuSe structures with triangular quantum wells⁸ and absorption measurements of PbSe/PbSrSe structures with parabolic quantum wells.¹² However, considerable discrepancies still remain among the experimental and theoretical data for the optical deformation potentials D_d and D_u . In particular, with a few exceptions,^{7,8,11} most D_d and D_u values do not agree with the isotropic (volume) deformation potential $D_{iso} = 3D_d + D_u$, determined with good accuracy from hydrostatic pressure experiments at different temperatures.^{7,8,13–15}

On the other hand, previous optical studies of IV–VI strained structures^{7–11} were based on the model that in these structures the lowest energy transition belongs to the normal (longitudinal) valley. Recent differential transmission spectroscopy of PbSe/PbSrSe/BaF₂(111) MQW structures clearly demonstrates this validity at well widths up to 30 nm.¹⁶ An important aspect of this work is that the authors¹⁶ were able to measure the intervalley splitting which results directly in one (D_u) of deformation potential constants and the next one (D_d) can be obtained from the D_{iso} relation.

Presented here is a detailed analysis of the absorption and PL spectra of high quality PbSe/PbSrSe and PbTe/PbEuTe MQW structures at different sample temperatures. Published data for PbTe/BaF₂ strained structures^{5,17,18} were also used. Based on the experimentally determined D_{iso} and the unambiguously determined well-width dependent intervalley splitting¹⁶ we have used a fitting procedure within an accu-

TABLE I. Acoustic ($D_d^{c,v}$ and $D_u^{c,v}$) and optical ($D_d=D_d^c-D_d^v$ and $D_u=D_u^c-D_u^v$) deformation potential values for the IV–VI semiconductors (in eV).

Material	D_d^c	D_u^c	D_d^v	D_u^v	$D_d^c-D_d^v$	$D_u^c-D_u^v$	D_{iso}	Reference
PbS	-3.60	5.01	-8.75	3.25	5.15	+1.76	17.21	Rabii ²²
		1.38		3.42		-1.94		Enders ²³
		6.9						Finlayson ²⁵
	-2.67	2.56	-9.15	4.67	6.48	-2.11	17.24	Rabii ²²
PbSe		1.06		3.14		-2.08		Enders ²³
					6.5	-3.7	15.8	Valeiko ⁸
					6.1	-1.3	17.0	Wu ¹²
					5.3	-0.2	15.7	4 K
					5.33	-0.6	15.4	77 K (this work)
					4.9	-0.7	14.0	300 K
PbTe	-4.36	8.29	-8.93	10.46	4.57	-2.17	11.55	Ferreira ²¹
		0.297		2.48		-2.18		Enders ²³
	-1.09	2.07	-2.23	2.62	1.14	-0.55	2.87	Kriechbaum ⁶
			4.9	5.4	1.9	-0.5	6 (5.2)	Singleton ⁵
					4.3	-2.8	10.1	Valeiko ^{7,8}
		± 0.5		0 or 1	3.53	-0.5	10.1	~ 4 K (this work)
		-5.5		-8		+2.5		Ilisavskii ²⁶
		3		9		-6		Shamshur ²⁷

rate two-band $\mathbf{k} \cdot \mathbf{p}$ model for the low energy transitions. This permitted the determination of new values for the PbSe and PbTe optical deformation potentials, which fit best the available data. Before the description of the experiments and the discussion of the results, we next briefly review the theory of IV–VI semiconductor quantum well energy level change due to uniaxial strain.

II. THEORY

For the present purpose, the deformation potential can be simply defined with the general expression for the band-edge energy shift due to strain, i.e.,

$$\delta E_{c,v} = \sum_{ij} D_{ij}^{c,v} \varepsilon_{ij}, \quad (1)$$

where $D^{c,v}$ is the conduction or valence band deformation potential tensor and ε is the strain tensor. The lead-salt band edge states at each of the four equivalent L points, except for Kramers degeneracy which is not removed with strain, are nondegenerate and, in the linear regime (or first order approximation), Eq. (1) is always valid. For these states, by cubic crystal symmetry, it is known that the deformation potential tensor is determined by only two independent constants, $D_d^{c,v}$ and $D_u^{c,v}$, the dilatation and uniaxial acoustic deformation potentials, respectively.¹⁹ In the 1960s, these deformation potentials have been calculated, with the augmented-plane-wave (APW) method based on the Pikus and Bir²⁰ strain Hamiltonian, for PbTe by Ferreira²¹ and for

PbSe and PbS by Rabii.²² Later on, Enders²³ performed tight-binding calculations based on the so-called p -model and got quite different values plus a sensible nonlinearity with the strain. In Table I, we have listed the obtained theoretical values (at very small distortion for Ref. 23) together with those obtained experimentally by different groups. The mentioned large variation is clearly seen and calls for both more calculations and measurements.

As given by Eq. (1), the strain energy shift depends on both deformation potential and strain tensors. If we consider only thin (under critical thickness) layers, i.e., pseudomorphic growth, we can assume homogeneous strain determined by the in-plane isotropic strain parameter²⁴

$$\varepsilon_{\parallel} = \frac{a_{\parallel}}{a} - 1, \quad (2)$$

where a is the substrate material lattice constant and a_{\parallel} is the common in-plane lattice constant of the epitaxial layer or MQW structure, which can be measured with good accuracy in a high resolution x-ray diffractometer. The only other strain component is the out-of-the-plane or perpendicular strain that is proportional to the in-plane strain,²⁴ i.e.,

$$\varepsilon_{\perp} = -2 \frac{C_{11} + 2C_{12} - 2C_{44}}{C_{11} + 2C_{12} + 4C_{44}} \varepsilon_{\parallel}, \quad (3)$$

with the proportionality constant given by the material elastic constants C_{ij} , which are known at different temperatures (see Ref. 28 for PbTe and Ref. 29 for PbSe).

TABLE II. Elastic constants, hydrostatic pressure gap coefficients, and D_{iso} values for PbSe and PbTe.

Material	PbSe			PbTe		
T , K	4	77	298	4	77	303
C_{11} , ^a 10^{10} N/m ²	14.18	13.98	12.37	12.81	12.43	10.80
C_{12} , ^a 10^{10} N/m ²	1.94	1.97	1.93	0.44	0.47	0.77
C_{44} , ^a 10^{10} N/m ²	1.749	1.695	1.591	1.514	1.482	1.344
$(C_{11}+2C_{12})$, ^a 10^{10} N/m ²	18.06	17.92	16.23	13.66	13.41	12.34
dE_g/dP , ^b 10^{-6} eV/bar	-8.7 ± 0.8	-8.6 ± 0.2	-8.6 ± 0.1	-7.4 ± 0.8	-7.4 ± 0.2	-7.5
D_{iso} , eV	15.7	15.4	14.0	10.1	9.9	9.3

^aElastic constants were taken from Refs. 28 and 29 for PbTe and PbSe, respectively.

^bThe pressure gap coefficients are taken from Refs. 7 and 8 at 4 K, from Ref. 14 at 77 K, from Ref. 13 for PbSe at 298 K, and from Ref. 15 for PbTe at 300 K.

The energy shift due to uniaxial strain in IV–VI semiconductors is different for the gap states at L points orientated differently with respect to the strain axis; and, therefore, the valley degeneracy of these materials can be lifted by uniaxial strain. In addition, the populations of different valleys may also be different. In optical experiments with uniaxially strained samples both the energy shift and the valley splitting are observable.

Let us consider in detail the typical and important examples of uniaxial strain due to lattice mismatch in epitaxial layers or MQW structures grown along the $[111]$ or $[100]$ crystallographic directions, as defined by common substrates for the growth of IV–VI materials. The different valleys in case of $[111]$ direction are divided into one orientated normally to the (111) plane in reciprocal space (i.e., along the $[111]$ growth direction) and three equivalent ones along directions forming the same angle with the growth direction, which are called oblique valleys. The interband optical transition energies probed in absorption and PL experiments depend only on the strain induced energy shift of the fundamental band gap E_g (and not on the valence and conduction band edge shifts independently). It is then convenient to define optical deformation potentials $D_d = D_d^c - D_d^v$ and $D_u = D_u^c - D_u^v$, so that the valley dependent energy gap strain shift is given by^{5,9}

$$\delta E_g^N = D_d(2\varepsilon_{\parallel} + \varepsilon_{\perp}) + D_u\varepsilon_{\perp} \quad (4)$$

and

$$\delta E_g^O = D_d(2\varepsilon_{\parallel} + \varepsilon_{\perp}) + D_u(8\varepsilon_{\parallel} + \varepsilon_{\perp})/9, \quad (5)$$

for the normal and oblique valleys, respectively. In Eqs. (4) and (5) the first term contributes to a shift in both the normal and oblique valleys by the same amount, while the second term contributes to a splitting of the two different valleys. The amount of this splitting depends only on the uniaxial deformation potential constant as follows:

$$\Delta = \delta E_g^N - \delta E_g^O = \frac{8}{9}D_u(\varepsilon_{\perp} - \varepsilon_{\parallel}). \quad (6)$$

In the case of $[100]$ -oriented substrates all four valleys are equivalent, i.e., all the major axes of the ellipsoids make the same angle with the surface normal. The gap change is given by

$$\delta E_g^{[100]} = \frac{2(C_{11} - C_{12})}{3C_{11}} D_{\text{iso}} \varepsilon_{\text{II}}. \quad (7)$$

Here the isotropic (volume) deformation potential D_{iso} is expressed through the optical deformation potentials as follows:³⁰

$$D_{\text{iso}} = 3D_d + D_u = -(C_{11} + 2C_{12}) \frac{dE_g}{dP}, \quad (8)$$

where dE_g/dP is the volume hydrostatic pressure gap coefficient.

For PbSe and PbTe, D_{iso} has been measured with good accuracy at room and low temperatures.^{7,8,13–15} The D_{iso} values are presented in Table II. In Fig. 1 we have plotted the empirical D_{iso} lines in the (D_u, D_d) space, for different tem-

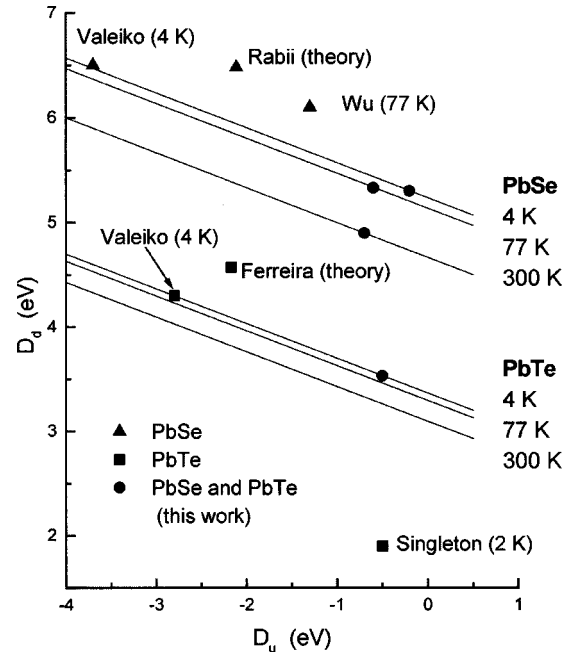


FIG. 1. Connection between dilatational and uniaxial optical deformation potential constants ($D_{\text{iso}} = 3D_d + D_u$) for PbSe and PbTe at different temperatures. The published theoretical and experimental D_{iso} values are very scattered around the straight lines.

peratures, and have assigned also the points corresponding to different independent determinations of D_u and D_d . The mentioned disagreement is clearly seen. For example, the measured D_{iso} value for PbTe^{5,6} is smaller by several times the value obtained from the pressure gap coefficient. The only data which obey the D_{iso} lines are the PL measurements.^{7,8,11} However they also need corrections due to the new absorption and PL data obtained with high quality deep quantum wells.

In MQW structures, the optical transition energies include also the addition of both electron and hole quantum size (or confinement) shifts, E_e and E_h , which besides being strongly well width dependent, can be calculated with high accuracy, especially for the lowest states, within the envelope function method based on a multiband $\mathbf{k} \cdot \mathbf{p}$ model for the bulk (with the band gap and the electron band edge effective mass, both eventually strain shifted, as the only parameters).³¹ Therefore, if the strain is known, the optical deformation potentials remain the only two unknown parameters in the evaluation of the quantum well optical transition energies.

Due to the strong well width dependence of quantum size energies and due to the intervalley splitting sign dependence, several different energy level structures can occur. When the quantum size shift is zero or small, as in thick epitaxial layers or wide quantum well structures, the strain induced valley splitting is accurately approximated by Eq. (6), i.e., depends only on D_u . In PbTe/PbEuTe and PbSe/PbSrSe MQW structures, the active quantum well PbTe and PbSe layers present in-plane tensile strain, i.e., $a_{||} > a$ and $\epsilon_{||}$ is positive. From Eqs. (3) and (6) it follows that if $D_u < 0$, Δ is, in this case, positive, meaning that the lowest optical transition in such an epitaxial layer or wide quantum well is from the oblique valleys. As the well width is reduced the confinement shifts for the oblique states increase much faster than that for the normal one (due to the much smaller oblique valley electron and hole effective mass along the growth direction); and, as a result, below a certain critical (crossing) well width the lowest transition is from the normal valley. Note that for $D_u > 0$, $|\Delta|$ increases monotonically with decreasing well width, and there is no crossing.

Such a crossing effect in strained PbSe quantum wells is illustrated in Fig. 2, where we have plotted the calculated lowest transition energies as a function of the well width for both normal and oblique valleys. A two-band model accounting for band nonparabolicity, many valley, and anisotropy effects is treated within the standard envelope function approximation. Since PL intensity for both MQW structures was high, comparable with one of the best thick (2–3 μm) epilayers grown on BaF₂ substrates, the heterojunction is of type-I. There is no information about band offsets for PbTe/PbEuTe and PbSe/PbSrSe heterojunctions. Considering the mirrorlike band structure of these materials and the good agreement obtained with the measured absorption spectra (including the 3 nm QW sample),⁹ we have used $\Delta E_c = \Delta E_v$ for our deep quantum wells ($\Delta E_g \geq 0.3$ eV at low temperatures), and checked that the lowest optical transition energies depend very little on deviations from such band edge discontinuities. Strain effects were also included with the energy gap and the effective masses renormalization in accordance with previous considerations and the two-band

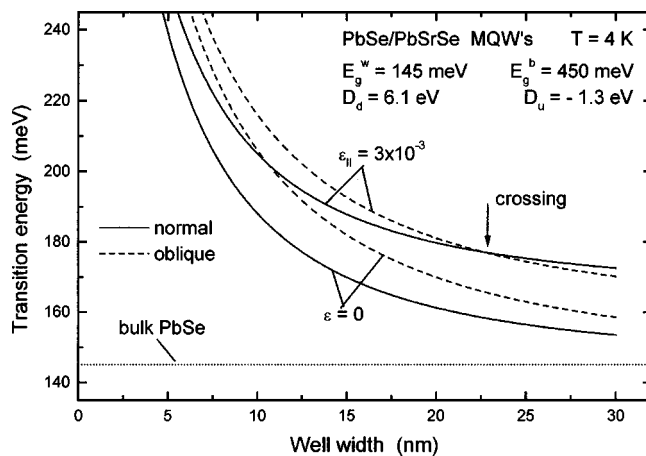


FIG. 2. Crossing of E_{11}^N and E_{11}^O interband transitions depending on the well width and strain for deformation potential values of $D_d=6.1$ eV and $D_u=-1.3$ eV.

model, respectively. The band edge effective masses for electrons and holes were taken from Ref. 32.

As we can see in Fig. 2, the energy spectrum of a quantum well is defined by quantum size and deformation effects. For narrow wells the quantum-size effect can be one order of magnitude larger than the deformation potential effect. For wide enough wells, instead, the deformation potential effect exceeds the quantum-size effect. At low temperature (4 K), a crossing PbSe well width of 23 nm is obtained with the deformation potentials reported in Ref. 12. With the values of Ref. 8 the crossing is seen to happen at a thinner well (~ 10 nm). However, this is in contradiction with the latest absorption observations:^{12,16,33} the energy of the normal valley transitions is always less than the energy of oblique valley transitions, at low temperatures and at well widths up to 30 nm. Therefore the optical deformation potential values should be reconsidered.

III. STRAIN

Due to different material constituents of a heterostructure, localized strain can occur and play an important role in the optical properties because of its influence on the transition energy. This problem is especially important in the case of IV–VI MQW structures using, as a rule, another material class as a substrate. There are two strain sources in IV–VI MQW structures grown on BaF₂ substrates. The first one is the lattice mismatch between structural constituents, i.e., between well and barrier. The structure growth is usually started on a relatively thick (i.e., relaxed) buffer layer and the well and barrier layers are thinner than the critical layer thickness, so in the first approximation they are elastically and uniformly strained. Since the lattice constants of PbEuTe and PbSrSe solid solutions (barriers) are larger than PbTe and PbSe (wells), respectively, the wells are under tensile in-plane strain and the barriers under compressive in-plane strain. However, as the number of repetitions in our MQW samples is high (40 to 50), the MQW stack does not remain pseudomorphic (same in-plane lattice constant) to the buffer

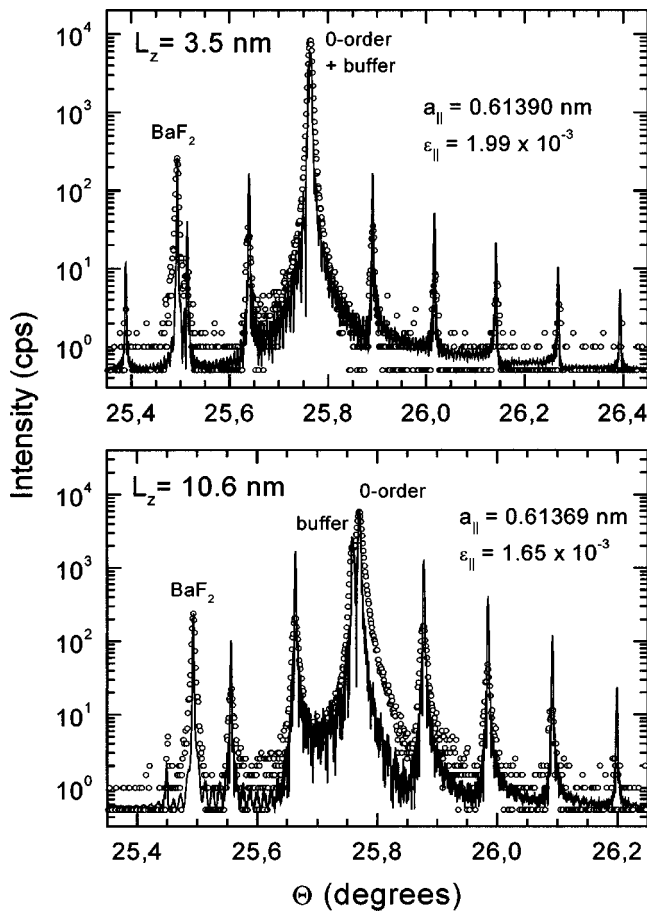


FIG. 3. $\omega/2\theta$ scan around the (222) Bragg diffraction peak for PbSe/PbSrSe MQW samples with PbSe well width of 3.5 nm (upper panel) and 10.6 nm (lower panel). The solid lines are the calculated spectra that best fit the measured data represented by the open circles.

layer. It starts to relax and tends to a free-standing condition. This fact becomes especially important as the well width increases. It was demonstrated for PbTe quantum wells in Ref. 34, where it was possible to fit the measured x-ray spectra of PbTe/PbEuTe MQW samples assuming a common in-plane lattice constant (different from the buffer value) for the whole MQW stack, and to determine the average strain in the PbTe wells. The fraction of the maximum parallel strain in the PbTe well decreased with the well width (by 26% at $L_z=20$ nm, see Fig. 5 in Ref. 34).

Similar strain analysis was done here for PbSe quantum wells. As an example, the $\omega/2\theta$ scan around the (222) Bragg diffraction peak is shown in Fig. 3 for the PbSe/PbSrSe MQW samples with PbSe well width of 3.5 and 10.6 nm. In both x-ray spectra, we can see the zero-order (most intense) plus several satellite peaks belonging to the MQW structure together with the BaF₂ substrate peak, which is used as a reference for the Θ axis. The PbSrSe buffer layer peak is overlapped by the zero-order peak in the x-ray spectrum of the sample with narrow PbSe well ($L_z=3.5$ nm) and the splitting between both peaks is already visible for the sample with larger wells ($L_z=10.6$ nm). In order to determine the strain inside the PbSe QW's, the (222) $\omega/2\theta$ spectrum of the

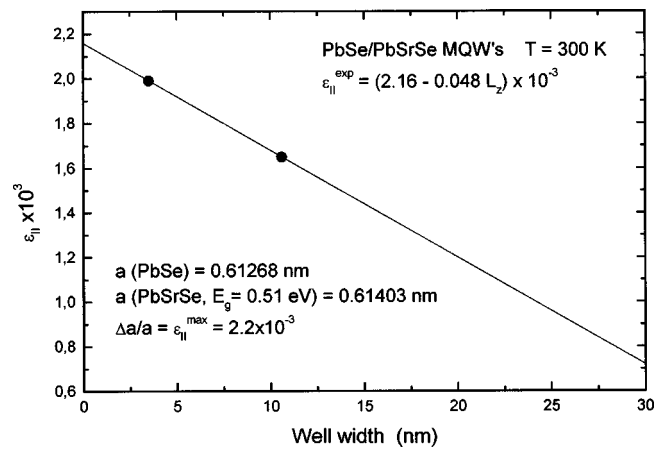


FIG. 4. In-plane strain ($\epsilon_{||}$) in the PbSe well of PbSe/PbSrSe MQW structures versus well width at 300 K.

MQW samples was calculated in the framework of dynamical theory of x-ray diffraction, and compared to the measured ones. The perpendicular strain component ϵ_{\perp} is obtained by Eq. (3) using elastic constants of the bulk material (Table II). The solid lines in Fig. 3 are the calculated spectra that best fit to the measured data (open circles), using the in-plane lattice constant ($a_{||}$) as the main fitting parameter. The parallel strain ($\epsilon_{||}$) in the PbSe wells of each sample was then determined using this fitting procedure and Fig. 4 shows how it varies with the well width. Thus, it is also necessary to take into account the well width strain dependence, and it is important for wide wells because the quantum size effect is still remarkable due to small effective masses in IV–VI semiconductors (see Fig. 2).

The second strain source is thermal expansion differences between the semiconductor structure and the substrate (in our case BaF₂). An important question concerning IV–VI epitaxial structures grown on the BaF₂ substrates arises: Is there a temperature at which this thermal strain is zero? The experimental evidence (electrical and optical properties) indicates that the strain is practically zero at room temperature. The x-ray diffraction measurements show that thick epilayers are almost unstrained at 300 K [the total residual strain is lower than 3×10^{-4} for a thickness of 5 μm (Ref. 35) or no strain to within $\pm 3 \times 10^{-5}$ (Ref. 36)]. This result is important since our previous x-ray measurements gave only the lattice mismatch strain at room temperature.

There are two possible reasons for the negligible thermal strain near room temperature. On cooling the samples from their growth temperature a stress is generated at the interface and it is relieved by creation and movement of dislocations. In addition, although the thermal expansion coefficients (α) of IV–VI semiconductors and the BaF₂ substrate are similar they do have a different temperature dependence:^{37,38} $\alpha(\text{IV-VI}) < \alpha(\text{BaF}_2)$ at growth temperatures of 350 °C and $\alpha(\text{IV-VI}) > \alpha(\text{BaF}_2)$ at temperatures less than ~ 100 °C. Thus, after sample cooling to room temperature, a partial compensation effect takes place.

On cooling the sample from room to cryogenic temperatures some residual elastic thermal strain in the sample is generated.³⁹ This is based on a study⁴⁰ where this thermal

strain in PbTe/BaF₂ films or PbTe/PbSnTe/BaF₂ superlattices was measured at low temperatures, and a value of 1.4×10^{-3} was obtained. The calculated³⁸ thermal strain between PbTe and BaF₂ is 1.6×10^{-3} , 1.4×10^{-3} , and 0.88×10^{-3} at temperatures of 4 K, 30 K, and 77 K, respectively. There is thus good agreement for a temperature of 30 K (the real sample temperature on the cold finger in the x-ray cryostat). These values should be added to the mismatched tensile strain values measured in the wells at room temperature. A similar analysis is needed for the PbSe/BaF₂ system. The direct $\Delta L/L_0$ temperature dependence for PbSe is not known, but it should have a temperature dependence of thermal expansion coefficient mismatch very close to that of PbTe.³⁷

IV. SAMPLES AND OPTICAL MEASUREMENTS

The PbSe/PbSrSe^{16,33} and PbTe/PbEuTe^{9,34} MQW structures used are briefly described here. They were grown on freshly cleaved BaF₂ (111) substrates by MBE at temperatures of 360 °C and 300 °C, respectively. Before growing the MQW structure a thick (3–4 μm) buffer with the same composition as the barriers was grown in order to accommodate completely the lattice mismatch of 1% and 4.4% for PbSrSe/BaF₂ and PbEuTe/BaF₂, respectively. The barrier composition was chosen to get a barrier band gap of 0.5 eV or more at 300 K as verified from infrared absorption measurements. Therefore, the wells were deep enough even at room temperature (at low temperatures ΔE_g increases due to the smaller gap temperature coefficient of the barrier materials³³). The well width was varied from 3 to 30 nm. The barrier thickness was varied from 40 to 50 nm. The number of periods was from 40 to 50.

The samples were characterized structurally by high resolution x-ray diffraction in the triple configuration to determine the barrier and well width lattice parameters.³⁴ Measurements were performed at room temperature. The strain in the wells inside the MQW structure was obtained as a function of its width using the common in-plane lattice constant as the main fitting parameter. It decreased monotonically with well width. MQW structures demonstrated a good resolved satellite peak structure that indicates their high quality (thickness reproducibility, homogeneous Eu or Sr content, and low interdiffusion).

Infrared transmission spectra were obtained at sample temperatures from 5 K to 300 K in a Fourier transform infrared spectrometer.^{9,16} PL spectra were measured in pulsed mode at 4 K and 77 K using a Nd:YAG laser ($h\nu = 1.17$ eV) for excitation and in CW mode at 300 K using an InGaAs laser ($h\nu = 1.28$ eV) for the excitation. A gold-doped germanium (7.5 μm cutoff wavelength) or HgCdZnTe (6 μm cutoff wavelength) detector with a detectivity of 10^{10} cm Hz^{1/2}/W was used. The energy resolution was 0.5–1 meV.

As-grown samples were used for the low temperature measurements. Therefore no deformation hardening took place² during several thermal cycles. Typical PL spectra of PbTe/PbEuTe MQW structures at 4 and 77 K are shown in Fig. 5(a). Emission lines are stimulated and they arise from the high energy side of spontaneous line, therefore, they rep-

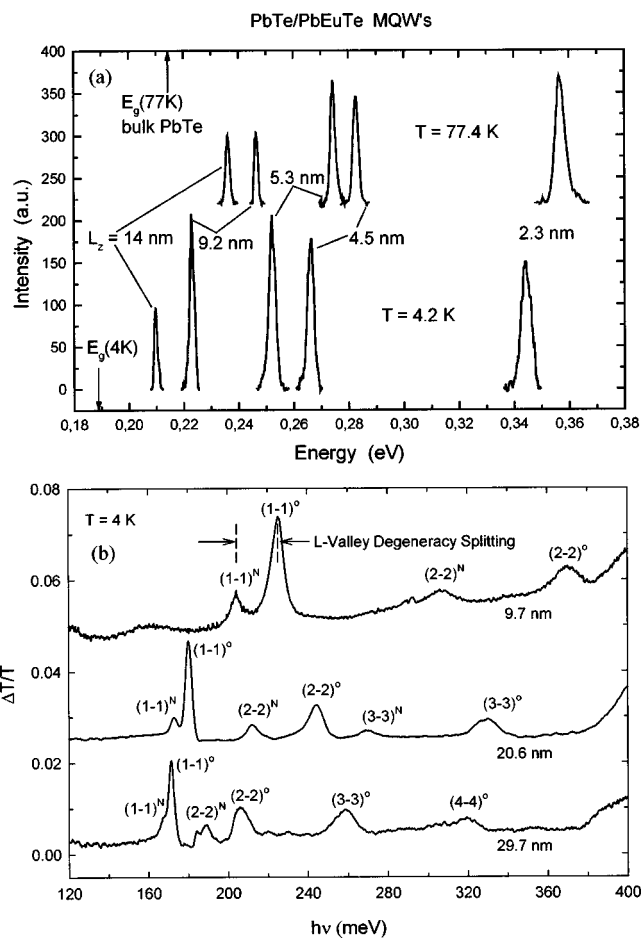


FIG. 5. The PL spectra of PbTe/PbEuTe MQW structures at 4 and 77 K (a) and derivative transmission spectra of PbSe/PbSrSe MQW structures at 4 K for different width PbSe wells (b).

resent with high accuracy the band gap. The PL linewidth was found to increase from approximately 1.5 to 4 meV as well width decreased from 20 to 2.3 nm at constant level excitation. It is due to penetration of quasi-Fermi levels into bands.

Typical differential spectra of PbSe/PbSrSe MQW structures with different well widths¹⁶ between 9.7 nm and 29.7 nm at 4 K are shown in Fig. 5(b). The spectra are obtained by taking the difference between a transmission spectrum at one temperature and the spectrum at a slightly lower temperature. This takes advantage of the temperature dependence of the PbSe band gap, so that step edges associated with different transitions in the transmission spectra become peaks in the difference spectra. Thus the temperature difference spectra are in essence energy derivative spectra. Splitting of *L*-valley degeneracy is indicated for the 9.7 nm thick QW. Note the remarkable peak intensity difference that reflects the different densities of states in normal and oblique valleys, i.e., transition intensity is much higher in the three-fold degenerate oblique valleys than in the one normal valley.

V. RESULTS AND DISCUSSION

As discussed above, depending mainly on the well width and on the specific values of the deformation potentials, the

TABLE III. Experimental and calculated valley splitting values for PbSe.

L_z (nm)	$\varepsilon_{\parallel} \times 10^3$	E_{11}^N (meV)	E_{11}^O (meV)	Δ_{calc} (meV)	Δ_{expt} (meV)
9.7	3.29	202.8	219.6	16.8	21.1
20.6	2.78	172.6	179.6	7.0	7.3
29.7	2.33	164.1	168.1	4.0	3.8

lowest optical transition in these QW structures can be either from the normal or from the oblique valleys. The corresponding transition energies are denoted by E_{11}^N and E_{11}^O , respectively, and given by $E_{11}^v = E_g + \delta E_g^v + E_{e,1}^v + E_{h,1}^v$, where $v=N, O$ and $E_{(e,h),1}^v$ is the first electron or hole quantized state from the v valley.

If we consider the pure strain effect for the [111] direction the following relation between the normal (E_{11}^N) and oblique valley (E_{11}^O) transition energies takes place: $E_{11}^N = E_{11}^O$ at $D_u = 0$; $E_{11}^N > E_{11}^O$ at $D_u < 0$; and $E_{11}^N < E_{11}^O$ at $D_u > 0$. The quantum-size effect increases both energies as the well width decreases. For example for PbSe, the E_{11}^O energy is blue-shifted twice as much as the E_{11}^N energy due to anisotropy effects, i.e., the transverse effective mass is almost one-half the longitudinal one. The final result of both energies depends on well width, effective mass, strain and deformation potential values.

In the first PL experiments^{7,8} the relation $E_{11}^N < E_{11}^O$ was used for the PbTe well widths up to $L_z = 20$ nm. Recent differential absorption spectroscopy results^{16,33} clearly demonstrate that the following relation takes place also in PbSe: $E_{11}^N < E_{11}^O$ at well widths up to 30 nm. The evaluations at $L_z = 30$ nm, where the level shifts due to quantum-size and deformation effects are comparable, show that the intervalley splitting $\Delta = E_{11}^N - E_{11}^O$ is relatively small. This means that D_u is negative and that level crossing takes place due to the quantum size effect. Using $D_u = -0.2$ eV we were able to get the calculated intervalley splitting very close to experimental values for three well widths at 4 K. The well strain for each MQW structure was determined as discussed above. The results are shown in Table III. For the fitting we used the calculated Δ values for the $L_z = 20.6$ nm and 29.7 nm [the large quantum-size contribution (~ 60 meV) at $L_z = 9.7$ nm is less accurately given by the present two-band model]. Imposing the D_{iso} constraint, we thus obtain $D_d = 5.3$ eV and $D_u = -0.2$ eV at 4 K. With these deformation potentials, we have calculated the transition energies at 4 K as a function of the well width and, as shown in Fig. 6(a), obtained very good agreement with the experimental data. To simplify, we have used an averaged (over samples) fixed strain of $\varepsilon_{\parallel} = 3 \times 10^{-3}$. In Fig. 6(b) we show the results at 77 K. In this case, we have used the intervalley splitting $\Delta = 5.5$ meV obtained at 66 K ($\varepsilon_{\parallel} = 2.18 \times 10^{-3}$). The best fit here leads to $D_u = -0.5$ eV and $D_d = 5.3$ eV. Along with the PL data at 77 K, we have plotted also the absorption data at 66 K. They are near 5 meV lower than the theoretical curves due to the PbSe temperature gap coefficient (0.4 meV/K). The second PL line corresponding to E_{22}^N transition was observed for sample $L_z = 10.6$ nm at a high excitation level ($\sim 10^5$ W/cm²).

Finally, the results at room temperature are plotted in Fig. 6(c). Since the intervalley splitting (~ 10 meV) for E_{11} transitions is small in comparison to kT at room temperature (26 meV) no differentiation between normal and oblique valleys is observed; most of the experimental points lay between the calculated curves. Thus good agreement was obtained between the low energy state differential spectroscopy and PL data, from one side, and the calculations in the framework of the two-band model, which is also valid for the low energy states, from the other side. It should be noted that the PbSe deformation potential values change with temperature: D_d slightly decreases and D_u by several times increases with increasing temperature (see Table I). Taking into account that D_d and D_u are differences of big quantities we can conclude that the acoustic potential values change with temperature.

The PbTe optical deformation potential constants were obtained (see below) from laser¹⁷ and magneto-optical^{15,18} measurements of PbTe/BaF₂ structures at low temperatures and they are $D_d = 3.53$ eV and $D_u = -0.5$ eV. We have used these values for calculation of quantum well transition energies which are compared with photoluminescence data for PbTe/PbEuTe MQW structures. Considering the previous evaluations of the thermal strain ($\varepsilon_{\parallel} = 1.6 \times 10^{-3}$ at 4 K and $\varepsilon_{\parallel} = 0.9 \times 10^{-3}$ at 77 K) and of the measured³⁴ mismatch strain (which depends on the well width and changes from 1.9×10^{-3} and 2.7×10^{-3}), we have used an averaged total strain of $\varepsilon_{\parallel} = 3.9 \times 10^{-3}$ and 3.2×10^{-3} at 4 K and 77 K, respectively. Calculations of the lowest (normal valley) transition energy at two temperatures are shown in Fig. 7. The photoluminescence data points are also presented. A rather good agreement between the two-band calculations with the new deformation potentials and the luminescence experimental data takes place.

As one can see in Figs. 6 and 7, some deviations between experimental and calculated transition energy values take place in the narrowest quantum wells ($L_z = 2.3$ and 3.5 nm for the PbTe/PbEuTe and PbSe/PbSrSe MQW's, respectively) due to the decreasing accuracy of the two-band model with increasing energy. For these high energy transitions the six-band mode^{5,6} should be used.

It should be noted that the obtained optical deformation potential constants for PbTe differ from most of the available data in the literature,^{7-11,21} except for the D_u value proposed in Ref. 5 and 6. It is very desirable to perform differential transmission spectroscopy measurements¹⁶ on high quality PbTe quantum wells. Next, we discuss the deformation energy shifts observed in different publications.

A. (100) Magneto-optical absorption

Interband magneto-optical absorption has been measured⁴ in epitaxial layers of PbS, PbSe, and PbTe grown on NaCl

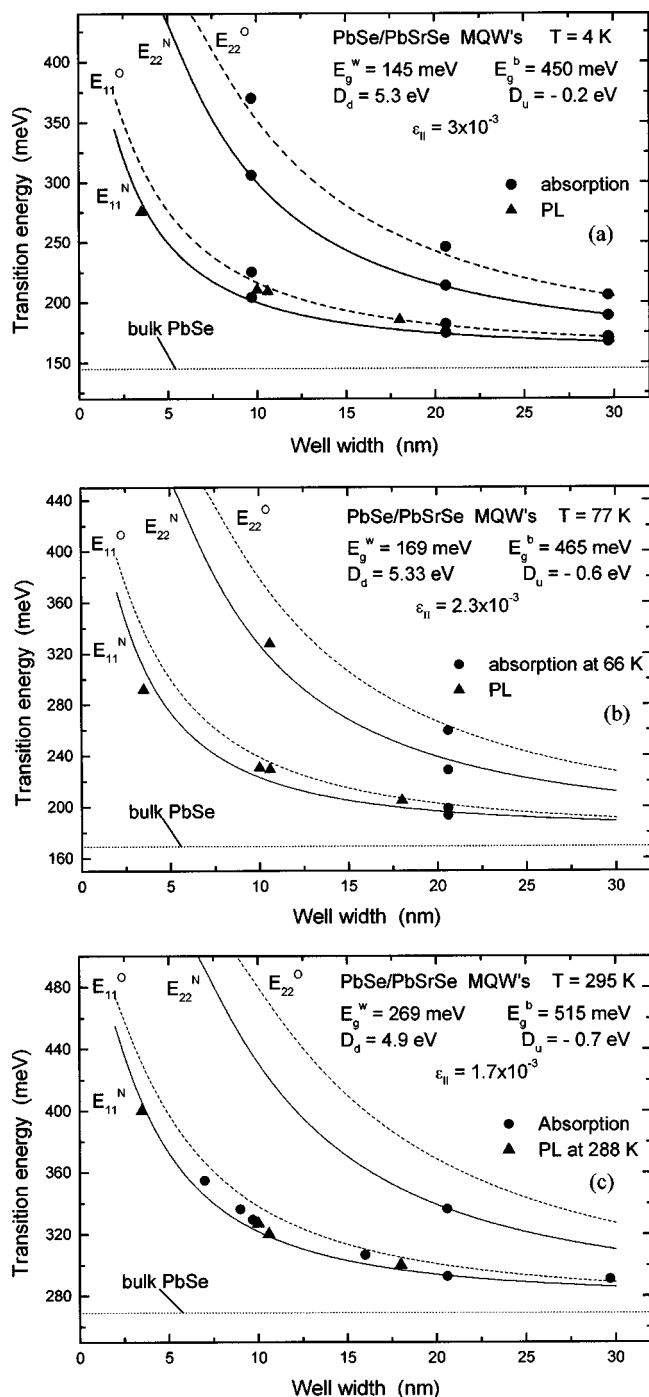


FIG. 6. Calculated sub-band transition energies versus well width of PbSe/PbSrSe MQWs at three temperatures: 4 K (a), 77 K (b), and 295 K (c). The solid and dashed lines correspond to transitions in normal (longitudinal) and oblique valleys, respectively. The deformation potential constants used are $D_d = 5.3$, 5.33, and 4.9 eV, and $D_u = -0.2$, -0.6 , and -0.7 eV; and the total averaged (over samples) strain is $\epsilon_{II} = (3, 2.3, \text{ and } 1.7) \times 10^{-3}$ at 4 K, 77 K, and 295 K, respectively. The PL data were obtained in pulsed mode at 4.2 and 77.4 K and in CW mode at 288 K.

(100) substrates. The layer thicknesses were 2–4 μm . The results are presented in Table IV. Our calculation was done using Eq. (7) for equivalent valleys. The thermal strain was taken from Ref. 38. We can see a good agreement between

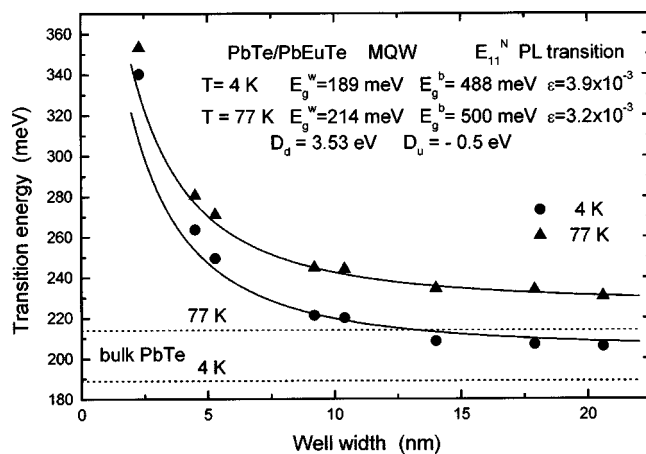


FIG. 7. Calculated lowest transition energies for normal (longitudinal) valley versus well width of PbTe/PbEuTe MQWs at 4 and 77 K. The deformation potential constants are $D_d = 3.53$ eV and $D_u = -0.5$ eV and the total averaged (over samples) strain is $\epsilon_{II} = 3.9 \times 10^{-3}$ and 3.2×10^{-3} at 4 K and 77 K, respectively. The PL data were obtained in pulsed mode.

calculated and measured δE_g . Agreement is even better for PbTe/NaCl if we compare the calculated value with the later measured shift values $\delta E_g = -17.5$ meV from an interband absorption study⁵ and $\delta E_g = -20$ meV from PL measurements.⁴¹ Some discrepancy is explained by the fact that the authors of Ref. 4 obtained anomalously high E_g (77 K) values for the free layers in the absorption measurements as compared to values which come from many laser and PL measurements, i.e., 169 and 214 meV for PbSe and PbTe, respectively.

B. (110) PbSe strained photoluminescence

Photoluminescence of a bulk PbSe(110) crystal under uniaxial pressure up to 150 bar at liquid helium temperatures was measured.³ A pulsed GaAs laser with the power of 5 W and pulse duration of 100 ns was used. Two emission lines were observed with slopes of $dh v_1/dP = 0.88 \times 10^{-5}$ and $dh v_2/dP = 2.17 \times 10^{-5}$ eV/bar. The photon energy at atmospheric pressure is $h\nu(P=1 \text{ bar}) = 161.9$ meV, which corresponds to a sample temperature of $T = 63$ K. The measured splitting value is $\Delta = 1.94$ meV at 150 bar. The calculated intervalley splitting for the [110] direction is: $\Delta = \delta E_g(111) - \delta E_g(\bar{1}\bar{1}\bar{1}) = 1.23 D_u \epsilon_{II}$. Using Young's modulus $E = 1.35 \times 10^5$ bar for PbSe at 77 K we obtain $\epsilon_{II} \sim 10^{-4}$ at a uniaxial pressure of 150 bar yielding a splitting value of only $\Delta = 0.06$ meV, which is more than one order of magnitude lower than the experimental value. The situation here is still not clear. One reason for the discrepancy can be the nonuniformity of the applied uniaxial pressure.

C. (100) PbSe heterostructure laser emission shift

Laser emission shift was observed⁴² for a double heterostructure laser with PbSe as the active region material and different confinement layers consisting of PbS, PbEuSe, or PbSrSe. The thickness of the active and confinement layers

TABLE IV. Measured from magneto-optical absorption and calculated energy shifts (δE_g) for [100] direction and at 77 K.

Parameter		PbS	PbSe	PbTe	Remarks
E_g (4 K), meV	free	286	165	190	Ref. 4
E_g (77 K), meV	free	307	176	217	
	strained	278	159	203	
δE_g (measured at 77 K), meV		-29	-17	-14	
Z_{vc}^p , eV		4.2	2.5	2.1	
A (in $\delta E_g = A \cdot D_{\text{iso}} \cdot \epsilon_{\text{II}}$) at 77 K		0.58	0.57	0.64	Our data
D_{iso} , eV		14.4	15.4	9.9	
$\epsilon_{\text{II}} \times 10^3$		3.2	3.0	3.1	
δE_g (calculated at 77 K), meV		-26.7	-26.0	-19.8	

were 0.5 and 2–4 μm , respectively. Heterostructures were grown by MBE on PbSe (100) substrates. Depending on the lattice mismatch the energy shift in comparison with a homojunction laser was observed in the range from 3 to 22 meV. The shift sign was negative for PbS confinement layers (lower lattice constant) and positive for PbEuSe and PbSrSe confinement layers (higher lattice constant). The energy shift for the strained PbSe (100) layer is $\delta E_g = 0.58 D_{\text{iso}} \epsilon_{\text{II}}$. The thermal strain is negligible for these related materials. Using the lattice mismatch [$\epsilon_{\text{II}} = (0.5 - 3) \times 10^{-3}$] as a strain we get $\delta E_g = 4.5 - 27$ meV. The measured shifts are slightly smaller than these calculated values, which is likely due to the partial misfit dislocation creation in the MBE-grown sample. In the case of PbS confinement layers the misfit dislocations dominate ($\Delta a/a \sim 3\%$) and only a redshift of 8 meV due to residual strain is observed.

D. (111) Splitting of the thin film PbTe laser emission

In Ref. 17 a splitting of 1.4 meV was observed in a thin film PbTe/BaF₂(111) laser at 9.5 K, in pulsed mode at injection currents well above threshold. The authors attributed this splitting to the relatively small strain of 2.2×10^{-4} in the laser material. However, this value contradicts the known strain of 1.6×10^{-3} in this structure at 4 K. The normal and oblique valley splitting is $\Delta = 1.85 D_u \epsilon_{\text{II}}$ at 4 K. Using $\epsilon_{\text{II}} = 1.6 \times 10^{-3}$ and $|D_u^c| = 0.5$ eV we obtain $\Delta = 1.5$ meV in accordance with the observed value.

The intensity of the low energy laser line is greater than that of the high energy laser line. This is consistent with the low energy laser line being due to oblique valley transitions and the high energy laser line being due to normal valley transitions, which is also in accordance with the magneto-optical finding.⁵ This results in $D_u < 0$. Now using D_{iso} (see Table II) we can evaluate the other deformation potential constant, $D_d = 3.5$ eV. The measured spectral position of the low energy line of a thin-film PbTe/BaF₂ laser is near 192 meV. The bulk PbTe band gap at 10 K is 189 meV, i.e., the gap difference between bulk PbTe and strained PbTe layer is 3 meV. On the other hand, we can calculate this gap difference (or the oblique valley shift) as $\delta E_g^O = (0.92 D_d$

$+ 0.77 D_u) \epsilon_{\text{II}}$. Using $D_d = 3.53$ eV, $D_u = -0.5$ eV, and $\epsilon_{\text{II}} = 1.6 \times 10^{-3}$ we obtain $\delta E_g = 4.5$ meV which is close to the measured gap difference (3 meV).

E. (111) PbTe magneto-optical studies

Interband⁵ and intraband¹⁸ magneto-optical low temperature studies were performed with strained epitaxial PbTe layers grown on BaF₂(111) substrates. Though authors in interband experiments⁵ have measured an intervalley splitting of only 0.9 meV after a fitting procedure they have obtained the same value of the uniaxial deformation potential $D_u = -0.5$ eV as we have evaluated from Ref. 17. An intervalley splitting energy of $\Delta^c = 1.5$ meV for intraband (conduction band) transitions was measured.¹⁸ The formula for intraband valley splitting is $\Delta^c = 1.85 D_u^c \epsilon_{\text{II}}$ which gives the acoustic deformation potential for the conduction band $|D_u^c| = 0.5$ eV at $\epsilon_{\text{II}} = 1.6 \times 10^{-3}$. Taking into account these values for D_u and D_u^c it is possible to conclude that the acoustic deformation potential for the PbTe valence band, D_u^v , is equal to 1 eV.

VI. CONCLUSIONS

Summarizing, with the use of measured strain induced intervalley splitting energies, empirical isotropic deformation potentials, and a detailed analysis of the strain we were able to determine new optical deformation potential values for PbSe and PbTe. At 4 K, for example, we have found $D_u = -0.2$ and -0.5 eV, and $D_d = 5.3$ and 3.5 eV for PbSe and PbTe, respectively. They result from the best fit to the photoluminescence and differential absorption spectroscopy data using an envelope function calculation based on an accurate two-band $\mathbf{k} \cdot \mathbf{p}$ model for the bulk. In general, but more specifically at low temperatures, a small uniaxial optical deformation potential constant (D_u) is obtained for both PbSe and PbTe due probably to the mirror symmetry of the conduction and valence bands in these materials.

ACKNOWLEDGMENTS

This work was supported in part by the National Science Foundation, Grant Nos. DMR-9802396 and DMR-0080054.

I.I.Z. was supported in part by Russian support program of the leading scientific schools No. SS-1923.2003.2. Financial support from CNPq and FARESP, Brazil, is also acknowledged.

- ¹Yu. I. Ravich, B. A. Efimova, and I. A. Smirnov, *Semiconducting Lead Chalcogenides*, edited by L. S. Stil'bans (Plenum, New York, London, 1970).
- ²P. Müller, H. Zogg, A. Fach, J. John, C. Paglino, A. N. Tiwari, M. Krejci, and G. Kosterz, *Phys. Rev. Lett.* **78**, 3007 (1997).
- ³G. W. Pratt, Jr. and P. G. McMullin, *Proceedings of the 10th International Conference on Physics Semiconductors* (Cambridge University Press, Cambridge, MA, 1970), p. 87.
- ⁴D. L. Mitchell, E. D. Palik, and J. N. Zemel, in *Physics of Semiconductors—Proceedings of the 7th International Conference, Paris, 1964*, edited by M. Hulin (Dunod, Paris, 1964), p.325.
- ⁵J. Singleton, E. Kress-Rogers, A. V. Lewis, R. J. Nicholas, E. J. Fantner, G. Bauer, and A. Lopez-Otero, *J. Phys. C* **19**, 77 (1986).
- ⁶M. Kriechbaum, K. E. Ambrosch, E. F. Fantner, H. Pascher, H. Clemens, and G. Bauer, *Phys. Rev. B* **30**, 3394 (1984).
- ⁷M. V. Valeiko, K. I. Geiman, I. I. Zasavitskii, A. V. Matveenko, and B. N. Matsonashvili, *Fiz. Tverd. Tela (Leningrad)* **33**, 1086 (1991) [*Sov. Phys. Solid State* **33**, 615 (1991)].
- ⁸M. V. Valeiko, I. I. Zasavitskii, A. V. Matveenko, B. N. Matsonashvili, and Z. A. Rukhadze, *Superlattices Microstruct.* **9**, 195 (1991).
- ⁹E. Abramof, E. A. de Andrada e Silva, S. O. Ferreira, P. Motisuke, P. H. O. Rappl, and A. Y. Ueta, *Phys. Rev. B* **63**, 085304 (2001).
- ¹⁰E. Abramof, E. A. de Andrada e Silva, I. I. Zasavitskii, S. O. Ferreira, P. Motisuke, P. H. O. Rappl, and A. Y. Ueta, *Physica E (Amsterdam)* **13**, 1224 (2002).
- ¹¹I. I. Zasavitskii, E. V. Bushuev, E. A. de Andrada e Silva, and E. Abramof, *JETP Lett.* **75**, 559 (2002).
- ¹²H. Wu, N. Dai, and P. J. McCann, *Phys. Rev. B* **66**, 045303 (2002).
- ¹³G. Martinez, *Phys. Rev. B* **8**, 4686 (1973).
- ¹⁴M. Schluter, G. Martinez, and M. L. Cohen, *Phys. Rev. B* **12**, 650 (1975).
- ¹⁵N. M. Ravindra and V. K. Srivastava, *Phys. Status Solidi A* **58**, 311 (1980).
- ¹⁶H. Z. Wu, N. Dai, M. B. Johnson, P. J. McCann, and Z. S. Shi, *Appl. Phys. Lett.* **78**, 2199 (2001).
- ¹⁷W. H. Weber and K. F. Yeung, *J. Appl. Phys.* **44**, 1991 (1973).
- ¹⁸J. Oswald, P. Pichler, B. B. Goldberg, and G. Bauer, *Phys. Rev. B* **49**, 17029 (1994).
- ¹⁹C. Herring and E. Fogt, *Phys. Rev.* **101**, 944 (1956).
- ²⁰G. E. Picus and G. L. Bir, *Fiz. Tverd. Tela (Leningrad)* **4**, 2090 (1962) [*Sov. Phys. Solid State* **4**, 1530 (1963)].
- ²¹L. G. Ferreira, *Phys. Rev.* **137A**, 1601 (1965).
- ²²S. Rabii, *Phys. Rev.* **167**, 801 (1968).
- ²³P. Enders, *Phys. Status Solidi B* **129**, 89 (1982); **132**, 165 (1985).
- ²⁴E. Anastassakis and M. Cardona, in *High Pressure in Semiconductor Physics II*, edited by T. Suski and W. Paul, *Semiconductors and Semimetals*, Vol. 55 (Academic, New York, 1998), p. 117.
- ²⁵D. M. Finlayson and A. D. Stewart, *Br. J. Appl. Phys.* **17**, 737 (1966).
- ²⁶Yu. V. Ilisavskii, *Fiz. Tverd. Tela (Leningrad)* **4**, 918 (1962) [*Sov. Phys. Solid State* **4**, 674 (1962)].
- ²⁷D. V. Shamshur, R. V. Parfen'ev, D. V. Mashovets, A. V. Matveenko, V. V. Kosarev, and K. I. Geiman, *Fiz. Tekh. Poluprovodn. (S.-Peterburg)* **16**, 1249 (1982) [*Sov. Phys. Semicond.* **16**, 798 (1982)].
- ²⁸B. Houston, R. E. Strakna, and H. S. Belson, *J. Appl. Phys.* **39**, 3913 (1968).
- ²⁹G. Lippmann, P. Kastner, and W. Wanninger, *Phys. Status Solidi A* **6**, K159 (1971).
- ³⁰J. F. Nye, *Physical Properties of Crystals* (Clarendon, Oxford, 1964).
- ³¹E. A. de Andrada e Silva, *Phys. Rev. B* **60**, 8859 (1999).
- ³²K. F. Cuff, M. R. Ellett, C. D. Kuglin, and L. R. Williams, in *Physics of Semiconductors—Proceedings of the 7th International Conference, Paris, 1964*, edited by M. Hulin (Dunod, Paris, 1964), p. 677.
- ³³H. Z. Wu, P. J. McCann, O. Alkhouli, X. M. Fang, D. McAlister, K. Namjou, N. Dai, S. J. Chung, and P. H. O. Rappl, *J. Vac. Sci. Technol. B* **19**, 1447 (2001).
- ³⁴E. Abramof, P. H. O. Rappl, A. Y. Ueta, and P. Motisuke, *J. Appl. Phys.* **88**, 725 (2000).
- ³⁵E. J. Fantner, B. Ortner, W. Ruhs, and A. Lopez-Otero, *Lecture Notes in Physics*, edited by E. Gornik, H. Heinrich, and L. Palmetshofer (Springer-Verlag, Berlin, Heidelberg, New York, 1982), Vol. 152, p. 59.
- ³⁶D. K. Hohnke and M. D. Hurley, *J. Appl. Phys.* **47**, 4975 (1976).
- ³⁷S. I. Novikova and N. Kh. Abrikosov, *Fiz. Tverd. Tela (Leningrad)* **5**, 1913 (1963) [*Sov. Phys. Solid State* **5**, 1397 (1964)].
- ³⁸Thermal expansion (nonmetallic solids). *Thermophysical Properties of Matter*, edited by Y. S. Touloukian, R. K. Kirby, R. E. Taylor, and T. Y. R. Lee (Plenum, New York, 1977), Vol. 13, pp. 1021 and 1250.
- ³⁹It was shown (Ref. 2) that the thermal mismatch strain in stacks containing the IV–VI semiconductor, BaF₂ and CaF₂ on Si(111) substrates is relieved by the glide of dislocations even at low temperatures. In the case of IV–VI semiconductors grown on BaF₂ substrates the thermal mismatch strain is one order of magnitude lower than in the case of layers grown on Si substrates. From the very beginning it results in high structural MQW quality (the dislocation density of 10⁶ cm⁻² and rocking curve XRD FWHM values <60 arc s). Dislocation climb can be responsible for this residual strain. Besides it is not clear if dislocations glide in the multiple deep quantum well materials systems with band offsets of ~0.2 eV.
- ⁴⁰E. J. Fantner, *Appl. Phys. Lett.* **47**, 803 (1985).
- ⁴¹J. W. Tomm, J. Griesche, H. Schmidt, D. Genzow, and J. Siemon, *Phys. Status Solidi A* **114**, 621 (1989).
- ⁴²H. Böttner, U. Schiessl, and M. Tacke, *Superlattices Microstruct.* **7**, 97 (1990).